Ni Yao[1], Yanhui Tian[1], Daniel Gama das Neves[2, 3], Chen Zhao[4], Claudio Tinoco Mesquita[2], Wolney de Andrade Martins[3, 5], Alair Augusto Sarmet Moreira Damas dos Santos[2, 3], Yanting Li[1], Chuang Han[1], Fubao Zhu[1], Neng Dai[6, 7], Weihua Zhou[4, 8]

[1] Zhengzhou University of Light Industry, School of Computer Science and Technology, Zhengzhou, Henan, China
[2] Universidade Federal Fluminense, Department of Radiology, Rio de Janeiro State, Brazil
[3] DASA Complexo Hospitalar de Niterói, Rio de Janeiro State, Brazil
[4] Michigan Technological University, Department of Applied Computing, Houghton, MI, USA
[5] Universidade Federal Fluminense, Department of Cardiology, Rio de Janeiro State, Brazil
[6] Zhongshan Hospital, Fudan University, Shanghai Institute of Cardiovascular Diseases, Department of Cardiology, Shanghai, China
[7] National Clinical Research Center for Interventional Medicine, Shanghai, China
[8] Center for Biocomputing and Digital Health, Institute of Computing and Cybersystems, and Health Research Institute, Michigan Technological University, Houghton, MI, USA

Incremental Value of Radiomics Features of Epicardial Adipose Tissue for Detecting the Severity of COVID-19 Infection

Introduction	Epicardial adipose tissue (EAT) is known for its pro-inflammatory properties and association with Coronavirus Disease 2019 (COVID-19) severity. However, existing detection methods for COVID-19 severity assessment often lack consideration of organs and tissues other than the lungs, which limits the accuracy and reliability of these predictive models.
Material and methods	The retrospective study included data from 515 COVID-19 patients (Cohort 1, n=415; Cohort 2, n=100) from two centers (Shanghai Public Health Center and Brazil Niteroi Hospital) between January 2020 and July 2020. Firstly, a three-stage EAT segmentation method was proposed by combining object detection and segmentation networks. Lung and EAT radiomics features were then extracted, and feature selection was performed. Finally, a hybrid model, based on seven machine learning models, was built for detecting COVID-19 severity. The hybrid model's performance and uncertainty were evaluated in both internal and external validation cohorts.
Results	For EAT extraction, the Dice similarity coefficients (DSC) of the two centers were 0.972 (±0.011) and 0.968 (±0.005), respectively. For severity detection, the area under the receiver operating characteristic curve (AUC), net reclassification improvement (NRI), and integrated discrimination improvement (IDI) of the hybrid model increased by 0.09 ($p<0.001$), 19.3% ($p<0.05$), and 18.0% ($p<0.05$) in the internal validation cohort, and by 0.06 ($p<0.001$), 18.0% ($p<0.05$) and 18.0% ($p<0.05$) in the external validation cohort, respectively. Uncertainty and radiomics features analysis confirmed the interpretability of increased certainty in case prediction after inclusion of EAT features.
Conclusion	This study proposed a novel three-stage EAT extraction method. We demonstrated that adding EAT radiomics features to a COVID-19 severity detection model results in increased accuracy and reduced uncertainty. The value of these features was also confirmed through feature importance ranking and visualization.

Keywords	COVID-19, epicardial adipose tissue, uncertainty, interpretability
For citations	Ni Yao, Yanhui Tian, Daniel Gama das Neves, Chen Zhao, Claudio Tinoco Mesquita, Wolney de Andrade Martins et al. Incremental Value of Radiomics Features of Epicardial Adipose Tissue for Detecting the Severity of COVID-19 Infection. Kardiologiia. 2024;64(9):96–104. [Russian: Ни Яо, Яньхуэй Тянь, Даниэль Гама дас Невес, Чэнь Чжао, Клаудио Тиноко Мескита, Вулни де Андраде Мартинс и др. Возрастающая роль радиомических особенностей эпикардиальной жировой ткани для выявления тяжести инфекции COVID-19. Кардиология. 2024;64(9):96–104].

Corresponding authors	Neng Dai, e-mail: niceday1987@hotmail.com. Weihua Zhou, e-mail: whzhou@mtu.edu

Introduction

The global health crisis sparked by the COVID-19 pandemic has underscored the importance of understanding the nuanced factors that influence the severity of the disease [1]. Initial investigations predominantly focused on pulmonary complications for severity assessment. However, recent attention has shifted towards exploring additional contributors, notably inflammation, and the pivotal role of epicardial adipose tissue (EAT) in disease progression [2].

Inflammation is a cornerstone in the trajectory of COVID-19, offering substantial insights into its severity as based on pulmonary findings [2]. EAT, located between

ISSN 0022-9040. Кардиология. 2024;64(9). DOI: 10.18087/cardio.2024.9.n2685

Central illustration. Incremental Value of Radiomics Features of Epicardial Adipose Tissue for Detecting the Severity of COVID-19 Infection

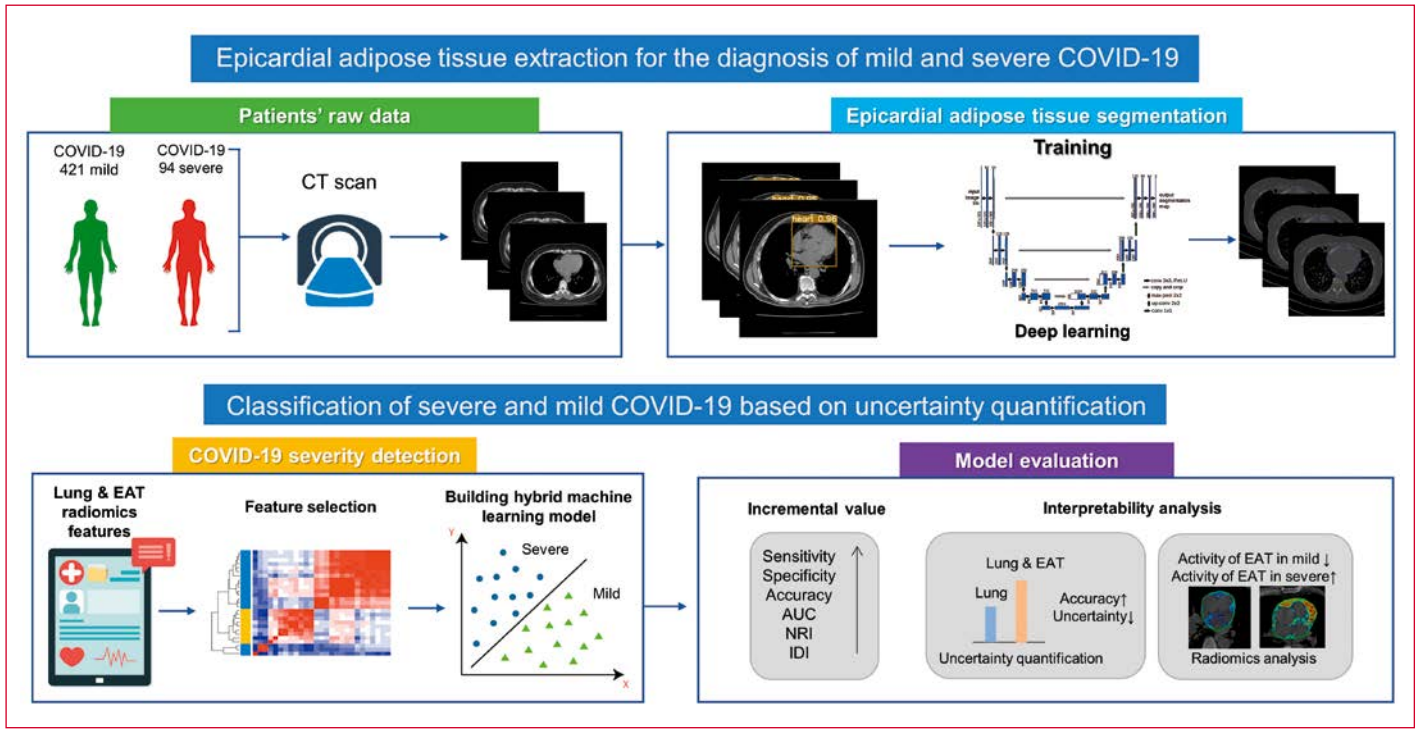

the myocardium and pericardium, is a significant source of pro-inflammatory mediators. This makes EAT an intriguing target for exploring the interplay between inflammation and disease severity [3]. The proximity of EAT to the coronary arteries and myocardium, coupled with its ability to secrete various anti-inflammatory and pro-inflammatory adipokines [4], links it closely with adverse cardiovascular events.

Studies have established a correlation between EAT volume and COVID-19 severity [5, 6], thus aiding in assessing the risk of disease progression. The evolving landscape of radiomics presents an opportunity to delve deeper into the intricate features of EAT, potentially uncovering novel insights into disease progression. However, traditional methods of EAT extraction are complex, laborious, and time-consuming, and these methods [7, 8] often lack consideration of EAT positional information.

Additionally, the reliability of predictive models in medical diagnostics is frequently questioned, necessitating robust methodologies for uncertainty quantification [9]. Integrating uncertainty into predictive models enhances interpretability and fosters trust in clinical decision-making.

This study hypothesized that EAT is significantly associated with the severity of COVID-19 infection. To address the shortcomings of existing EAT extraction methods, we proposed a novel, three-stage, automatic EAT extraction method. To investigate the incremental value of EAT features for the diagnosis of COVID-19 severity, we built a hybrid diagnostic model and evaluated its performance based on radiomics features and uncertainty analysis. This research has the potential to provide valuable insights into the role of EAT in COVID-19 severity and to enhance the overall understanding of the disease.

Material and methods

Study population

The retrospective study included patients treated at two medical centers between January and July, 2020 (Figure 1). There were 415 consecutive patients (371 mild and 44 severe cases) with confirmed COVID-19 at Shanghai Public Health Center (Cohort 1) [2] and 100 consecutive patients (50 mild and 50 severe cases) with confirmed COVID-19 cases at Brazil Niteroi Hospital (Cohort 2). The population division for each stage is in the supplementary material.

This study was approved by the Ethics Committees of the Shanghai Public Health Clinical Center and the Brazil Public Health Clinical Center.

Lung Segmentation

The lung segmentation was achieved according to the research method of Zhao et al. [10], and the segmentation results of lung were confirmed by radiologists. Unachieved lung segmentation results due to imaging difference segmentation were defined as unsatisfactory results. To ensure the accuracy of feature extraction, unsatisfied results were re-annotated manually by LabelMe software for lung.

Automatic Extraction of EAT

The method for the automatic extraction of EAT is structured into three main modules, each serving a specific

Figure 1. Flowchart of patient inclusion and exclusion and flowchart of modeling

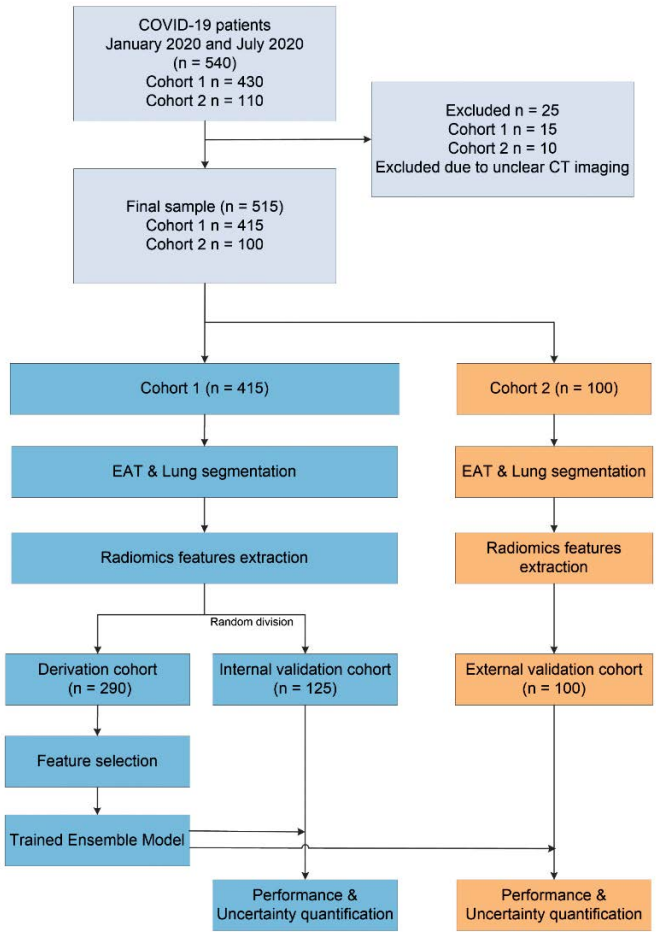

function in the segmentation process. The process is illustrated in Figure 2. Firstly, object detection is used as a guiding module in the initial stage to obtain positional information, which contributes to improved accuracy in subsequent segmentation. Following this, the results from object detection are then leveraged to conduct binary segmentation of the heart, distinguishing between the myocardium and endocardium, as well as the background. This step is carried out within the segmentation network, ultimately producing the contour of the heart. Finally, the third stage involves the implementation of thresholding and smoothing techniques within the heart contour to isolate and extract the EAT.

Object Detection

To address the time-consuming, manual screening of heart start and end frames of each patient, object detection is incorporated as a guide module to enhance the efficiency of heart segmentation. The YOLO-V5 network [11] is utilized for object detection, with the training samples consisting of images containing the heart. The input image size for the YOLO-V5 network is set to 512×512×1 px, and the corresponding labels include the normalized coordinates of the heart centroid (horizontal and vertical) within the image, as well as the width and height of the heart region. By passing the image through this bootstrap module, the network can output information regarding the heart's location. If the image contains the heart region, it will be identified as such; otherwise, it will be classified as not containing the heart region. This step enables automatic screening of images to identify those that contain the heart region for each patient.

Heart Segmentation

To achieve more accurate determination of the EAT range, a deep learning network was employed to automatically segment the heart contour in each patient image, before proceeding with the extraction of EAT. The heart contour segmentation model utilized in this study is based on the well-established U-Net network [12]. The U-Net network is a two-dimensional model with an input image size of 512×512×1 px. Upon processing an input image, it produces an output in the form of a probabilistic map that represents the heart contour. In this map, a value of 1 indicates the presence of the heart contour and its internal regions, while 0 represents the background. This step ensures the precise delineation of the heart structure, thereby facilitating the subsequent extraction of EAT.

Figure 2. Flowchart of EAT extraction

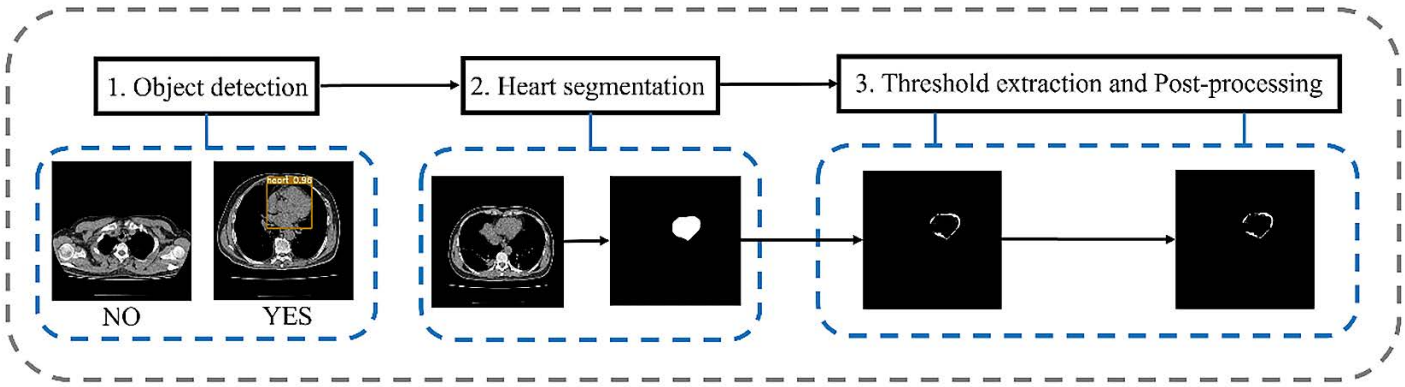

ISSN 0022-9040. Кардиология. 2024;64(9). DOI: 10.18087/cardio.2024.9.n2685

Threshold Extraction

As used in the generation of the reference, the threshold for adipose tissue has been defined as a Hounsfield Unit (HU) of –190 HU to –30 HU. EAT was obtained by threshold extraction and median filtering in the heart contour results obtained from the segmentation network.

Severity Detection

CT radiomics Features Extraction

In cohort 1 and cohort 2, each patient's lung and EAT regions were formed into three-dimensional images, and 120 radiomics features [13] of both lung and EAT were extracted, respectively.

Feature Selection

In the derivation cohort, univariate analysis and Pearson correlation analysis were used to identify predictors of COVID-19 severity classification from 120 lung and 120 EAT radiomics features. This analysis process was performed according to Zhao et al. [10]. Univariate logistic regression analysis was used to select features with significant differences. Then Pearson correlation analysis between features was conducted and strong correlation features were excluded with the selection threshold combined with the final number of included features.

Classification Model Modeling

In the derivation cohort (n=290), a hybrid model based on seven basic machine learning models was built. The basic machine learning models included Logistic Regression (LR) [14], Support Vector Machine (SVM) [15], Random Forest (RF) [16], Adaptive Boosting (AdaBoost) [17], Extreme Gradient Boosting (XgBoost) [18], Light Gradient Boosting Machine (LGBM) [19], and Gradient Boosting Decision Tree (GBDT) [20]. The hybrid model utilized the mean value of the predictions of the basic models as its prediction result, and the standard deviation of the predictions of the basic models was used as the uncertainty quantization of the prediction result.

The performance improvement of the COVID-19 severity classification model was subsequently validated using lung and EAT radiomics features in both an internal validation cohort (n=125) and an external validation cohort (n=100). The interpretability of the model was analyzed based on the radiomics features and the uncertainty quantization.

The uncertainty of prediction results was quantified into six levels ranging from 0 to 0.1, 0.1 to 0.2, 0.2 to 0.3, 0.3 to 0.4, 0.4 to 0.5, and 0.5 to 1. A lower uncertainty quantification value closer to 0 indicated a higher confidence in the model's prediction, while a value closer to 1 represented higher uncertainty and less confidence in the model's prediction. The uncertainty quantification results of the hybrid model combining radiomic features of both lung and EAT were evaluated in terms of their quantification levels in the internal validation cohort and external validation cohort, respectively.

Results

Patient Characteristics

In the derivation cohort, 30 (10.34%) patients were diagnosed with severe COVID-19. The mean age of mild and severe cases was 40.0±15.4 and 59.0±14.9, respectively, and 48% (n=260) and 53% (n=30) were male, respectively. The baseline characteristics of the patients in the derivation cohort are displayed in Supplementary Table 1. There were no significant differences (p>0.05) in gender, white blood cell count, potassium, and lactic acid. In Cohort 1, patients with respiratory symptoms of fever and pneumonia on imaging were diagnosed as having mild infection. Severe COVID-19 infection was defined by any of the following: shortness of breath with respiratory rate (RR) ≥30/min, pulse oxygen saturation (SpO_2) ≤93% at rest, arterial partial pressure of oxygen (PaO_2)/O_2 fraction of inspired oxygen (FiO_2) ≤300 mm Hg (adjusted for altitude), or significant clinical and lung lesion progression (>50% within 24–48 hrs) [21]. In Cohort 2, patients who only required treatment in the emergency department were diagnosed as mild infection, and patients admitted to the ICU and infirmary were diagnosed as severe infection.

EAT Extraction

The results, as presented in Table 1, demonstrate that the segmentation method employing YOLO-V5+U-Net outperforms existing methods significantly. The U-Net network predicted all images as background, with a resulting

Table 1. Comparisons of DSC and HD determined by different methods as applied to the two cohort test sets

	Method	DSC	HD (mm)
Cohort 1	U-Net	0.629±0.047	–
	V-Net	0.921±0.019	14.446±3.143
	Hoori et al. [7]	0.935±0.021	13.842±3.486
	Commandeur et al. [8]	0.943±0.016	10.548±3.042
	Yolo-V5 + U-Net (current method	0.972±0.011	7.538±2.112
Cohort 2	U-Net	0.653±0.032	–
	V-Net	0.903±0.024	17.169±5.168
	Hoori et al. [7]	0.925±0.022	14.846±3.744
	Commandeur et al. [8]	0.937±0.018	12.325±4.894
	Yolo-V5 + U-Net (current method	0.968±0.005	6.423±1.842

DSC, dice similarity coefficient; HD, Hausdorff distance.

Figure 3. Comparisons of the results of EAT extraction based on expert segmentation (left column), automatic heart segmentation by Yolo-V5+U-Net method (middle column, DSC=0.972), and automatic heart segmentation by V-Net method (right column, DSC=0.921) in Cohort 1

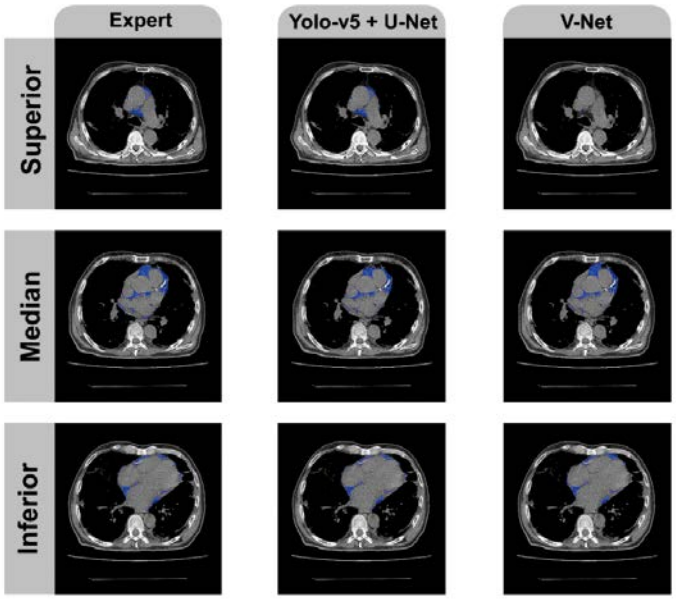

The blue area is EAT. The upper, middle, and lower rows correspond to the upper, middle, and lower parts of the heart.

DSC of 0.629. This led to all prediction results being negative samples, making it impossible to calculate HD. Visual comparison between EAT segmentation results annotated by experts and those predicted by the model is illustrated in Figure 3.

Figure 4. Top 20 feature importance scores

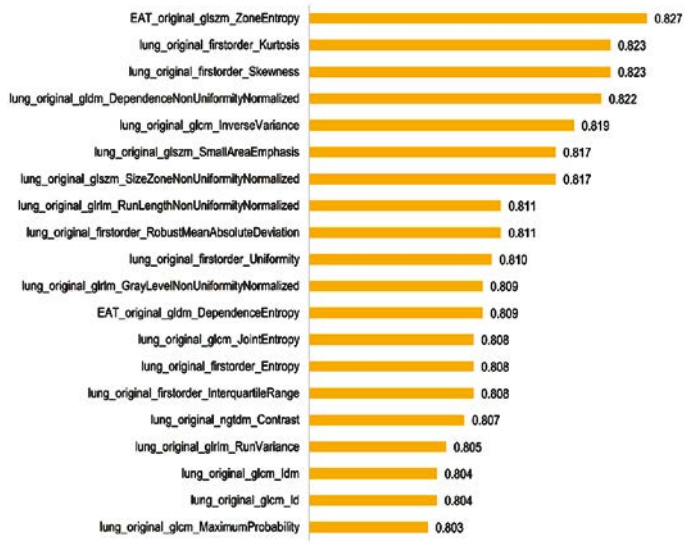

The left side of the bar shows the name of each feature, and the right side of the bar shows the feature importance score of the corresponding feature.

Table 2. Model fitting and calibration in the derivation cohort (n = 290) and the predictive performance of the internal validation cohort (n=125) and the external validation cohort (n=90) for the mild and severe classification

Cohort	Features	SN	SP	AUC	ACC
Internal Validation	Lung	0.786	0.910	0.867	0.896
	Lung+EAT	0.857	0.928	0.957	0.920
External Validation	Lung	0.742	0.847	0.851	0.810
	Lung+EAT	0.806	0.915	0.911	0.880

ACC, accuracy; AUC, area under the receiver operating characteristic curve; SN, sensitivity; SP, specificity.

Feature Selection and Diagnostic Model

120 radiomics features were extracted from lung and EAT, respectively. Feature selection was performed in the derivation cohort. 75 lung and 42 EAT radiomics features were significantly different in the severity classification. The order of feature selection was ranked from high to low according to the AUC score of the univariate analysis. The top 20 features and their importance scores are shown in Figure 4. The full features are shown in Supplementary Figure 1. The features with strong correlations were eliminated by correlation analysis among features (the correlation coefficient threshold was 0.75 in this paper). Finally, the remaining 6 lung radiomics features and 4 EAT radiomics features were included to build the diagnostic model (Supplementary Table 2).

Model performance in the validation cohort

Table 2 and Figure 5 shows the model performance for mild and severe classification in the internal and external validation cohort. In the internal validation cohort compared with the hybrid model with only lung features, the hybrid model with lung and EAT radiomics features demonstrated improved predictive efficacy; its NRI increased by 19.3% ($p<0.001$), and IDI increased by 18.0% ($p<0.001$). In the external validation cohort, the hybrid model with radiomics features of both lung and EAT demonstrated improved predictive performance; its NRI increased by 18.0% ($p<0.001$), and IDI increased by 18.0% ($p<0.001$).

What is more noteworthy is that regardless of the model, the performance of the model combining lung and EAT radiomics features was superior to the model with only lung radiomics features, which further validated the incremental value of EAT for COVID-19 severity detection.

Furthermore, a comparison was made with existing methods for COVID-19 severity diagnosis, as shown in Table 3. These studies employed different metrics to establish diagnostic models, including clinical features, radiological features of the lungs, and CT quantitative scores. Our method achieved optimal performance by incorporating radiomics features of both the lung and EAT.

ISSN 0022-9040. Кардиология. 2024;64(9). DOI: 10.18087/cardio.2024.9.n2685

Discussion

This study evaluated a fully automated EAT extraction method and the value of EAT radiomics features for severity stratification in COVID-19 patients. Main findings: 1) a three-stage method is proposed to improve the accuracy of EAT extraction, 2) the EAT radiomics features combined with lung have incremental value in detecting the severity of COVID-19 infection, and 3) the addition of EAT radiomics features provides improved interpretability and more confident predictions of results based on the hybrid model.

COVID-19 Severity Detection

In the study of the artificial intelligence detection severity of COVID-19 infection, Zhang et al. [24] used machine learning to classify patients' blood indicators for mild and severe cases of COVID-19. The naïve Bayes model was the best with an AUC of 0.90. Li et al. [25] had an AUC of 0.918 for mild and severe classification of CT visual quantitative score of patients. However, acquiring clinical indicators takes time, and the increase in diagnosis time may lead to delaying or missing the best treatment. At the same time, these methods lack interpretable analysis, and the

Figure 5. AUC plots for Hybrid models with lung and EAT radiomics features in internal and external validation cohort

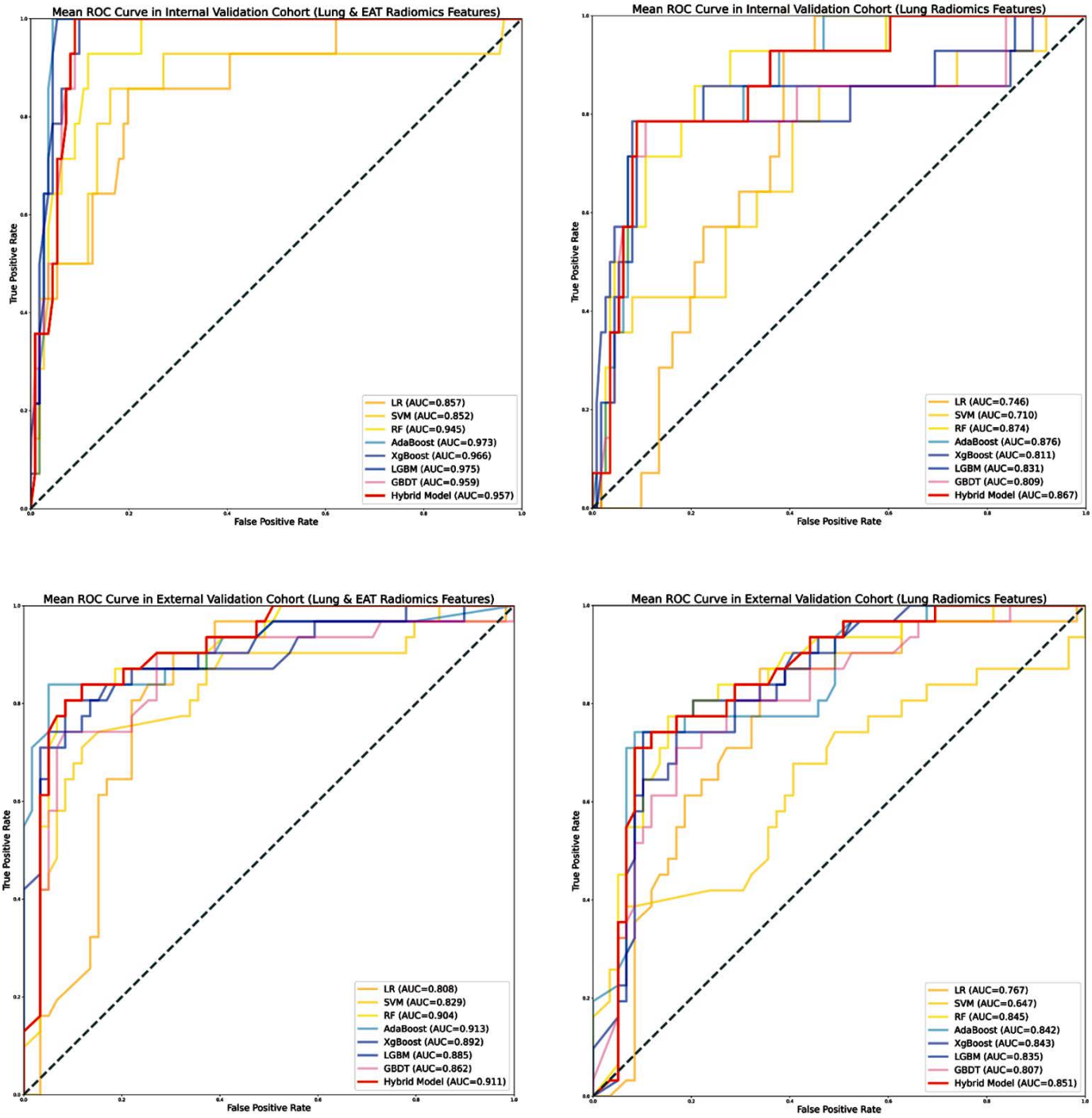

Table 3. Model performance comparison with state-of-the-art Covid-19 severity diagnosis methods

Method	Features	Number of patients	AUC	ACC
Liang et al. [22]	Clinical	1590 (131 severe)	0.88	–
Zhu et al. [2]	Clinical+ Lung radiomics	427 (40 severe)	0.94	0.93
Zhao et al. [23]	Clinical	172 (60 severe)	–	0.91
Zhang et al. [24]	Clinical	422 (102 severe)	0.90	–
Li et al. [25]	CT visual quantitative	78 (8 severe)	0.92	–
Current method	Lung + EAT radiomics	415 (44 severe)	0.96	0.92

ACC, accuracy; AUC, area under the receiver operating characteristic curve.

model cannot express whether it is confident about the predicted results and whether it can play the role of auxiliary diagnosis.

In addition, diagnostic methods that rely on imaging features only focusing on the lung region lack comprehensive judgment. COVID-19, especially in severely ill patients, may lead to complications in other parts of the patient's body. The heart has been confirmed to be one of the leading organs for such complications in previous studies [1]. Therefore, the detection of cardiac effects of COVID-19 should also be used as a factor for severity stratification. This would provide increased possibilities for more accurate stratification of COVID-19. As in previous studies [5, 6], EAT was found to be related to the severity of COVID-19 in terms of severity stratification. In this study, the incremental value of radiomics features of EAT integrated with lung for detecting COVID-19 severity was found and demonstrated in internal and external validation cohorts. Other mainstream classification models had also verified the incremental value of EAT for the classification of mild and severe. In addition, our analysis included more radiomics features of EAT, and we found other meaningful features which were not found in previous studies.

Interpretability Analysis

Based on Radiomics Features

The feature selection process identified ZoneEntropy and Skewness as essential features for characterizing EAT. These features reflect the uncertainty or randomness in the size and the gray distribution of the measurement area and the asymmetry of the value distribution. The adipose tissue attenuation value in EAT has a dynamic range [–190, –30], and these features highlight the instability of the adipose tissue attenuation value in the EAT region of the image. Figure 6 compares the EAT attenuation index between mild and severe COVID-19 patients, and it shows that this index was more unstable and closer to –30 HU in severe patients. This observation provides a more intuitive reflection of the association between EAT and COVID-19 severity. Previous studies [26] have shown that adipose tissue can influence inflammation, and this study hypothesized that COVID-19 affects EAT in severely ill COVID-19 patients, leading to increased adipose tissue activity. These findings explain the uncertainty in gray distribution and the asymmetry of value distribution in the EAT radiomics features.

Figure 6. EAT attenuation heatmaps for COVID-19 patients of different severity. The green contour represents the outline of the heartand external validation cohort

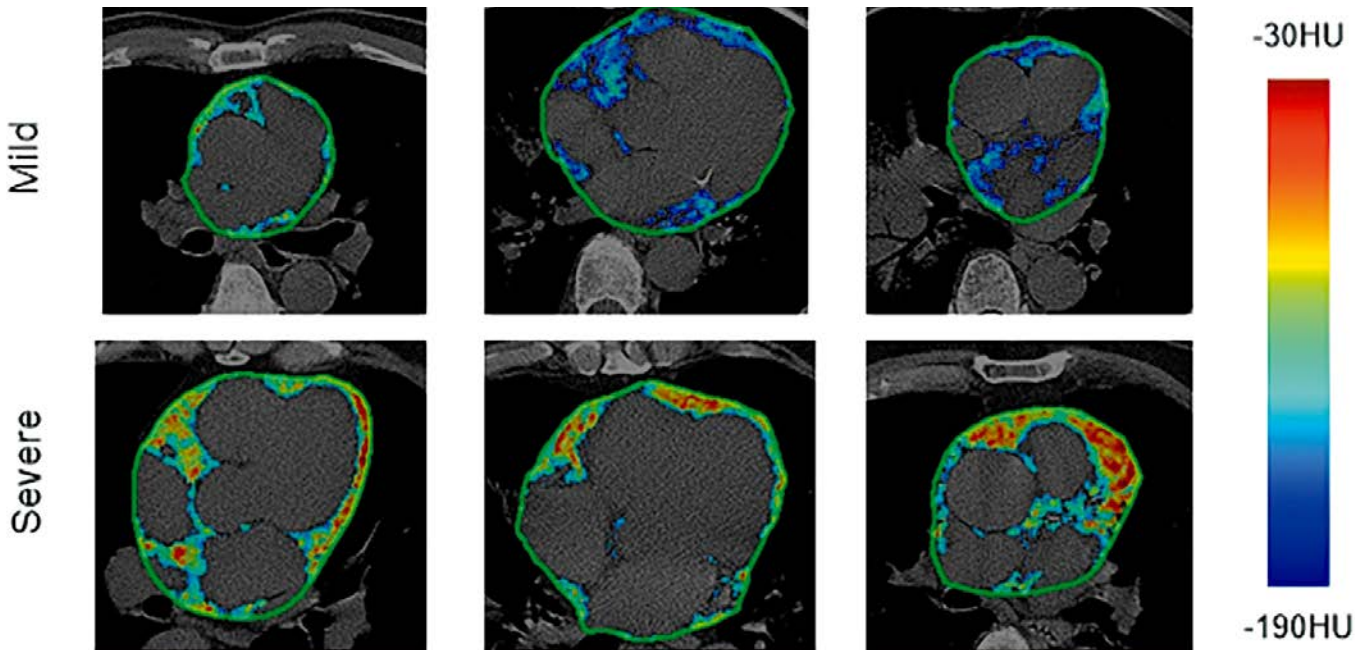

ISSN 0022-9040. Кардиология. 2024;64(9). DOI: 10.18087/cardio.2024.9.n2685

Figure 7. Comparison of quantified degrees of uncertainty between the hybrid model of lung radiomics features and the hybrid model of radiomics features of both lung and EAT in internal and external validation cohorts

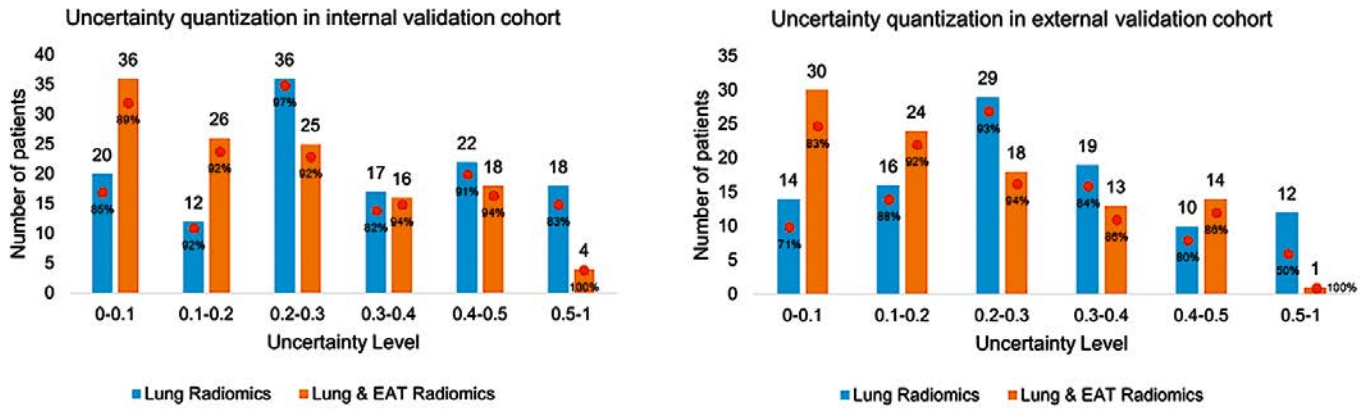

The red dots are the prediction accuracy of each level.

Uncertainty Quantization

Figure 7 illustrates the uncertainty quantification of results in the two validation cohorts. Compared to the hybrid model using lung radiomics features, the hybrid model incorporating both lung and EAT radiomics features exhibited a concentration of uncertainty in the ranges of 0–0.1 and 0.1–0.2, with higher accuracy within this range. This indicates that incorporating EAT radiomics features into the model enhances the confidence level and improves the accuracy of predicting the severity of the disease. This may be attributed to the inclusion of EAT radiomic features that likely capture additional characteristics related to the disease progression or to the underlying physiological factors that influence the severity of the condition. Additionally, it is noteworthy that the number of patients with uncertainty quantification between 0.5 and 1 was lower in the hybrid model that used both lung and EAT radiomics features as compared to the model using only lung radiomics features. Uncertainty values exceeding 0.5 indicate that the hybrid model cannot provide more stable and confident predictions, thus necessitating secondary decision-making by physicians. This also means that more secondary decision-making interventions by physicians were required for cases with high uncertainty values. Therefore, incorporating EAT radiomic features not only enhanced the efficiency of clinical workflow, but it also suggested the potential for targeted interventions and personalized treatment strategies based on the model's predictions and with additional insights from EAT radiomic features. A discussion of the EAT segmentation is included in the supplementary material.

Conclusions

In this study, we proposed a novel, three-stage EAT extraction method that surpasses existing methods in accuracy and efficiency. By utilizing a machine learning model integrated with uncertainty quantification, we have demonstrated the incremental value of EAT radiomics features in assessing the severity of COVID-19 infection. Specifically, adding EAT radiomics features to the COVID-19 severity detection model results in increased accuracy and reduced uncertainty. The value of these features is also confirmed through feature importance ranking and visualization.

Acknowledgments

This study received support from the National Natural Science Foundation of China (Grant Numbers: 62106233, 62303427, and 82370513), and the Henan Science and Technology Development Plan (Grant Number: 232102210010, 232102210062).

No conflict of interest is reported.

The article was received on 22/04/2024

REFERENCES

1. Long B, Brady WJ, Koyfman A, Gottlieb M. Cardiovascular complications in COVID-19. The American Journal of Emergency Medicine. 2020;38(7):1504–7. DOI: 10.1016/j.ajem.2020.04.048
2. Zhu F, Zhu Z, Zhang Y, Zhu H, Gao Z, Liu X et al. Severity detection of COVID-19 infection with machine learning of clinical records and CT images. Technology and Health Care. 2022;30(6):1299–314. DOI: 10.3233/THC-220321
3. Nalliah CJ, Bell JR, Raaijmakers AJA, Waddell HM, Wells SP, Bernasochi GB et al. Epicardial Adipose Tissue Accumulation Confers Atrial Conduction Abnormality. Journal of the American College of Cardiology. 2020;76(10):1197–211. DOI: 10.1016/j.jacc.2020.07.017
4. Feng X, Li S, Sun Q, Zhu J, Chen B, Xiong M et al. Immune-Inflammatory Parameters in COVID-19 Cases: A Systematic Review and

Meta-Analysis. Frontiers in Medicine. 2020;7:301. DOI: 10.3389/fmed.2020.00301
5. Kim I-C, Han S. Epicardial adipose tissue: fuel for COVID-19-induced cardiac injury? European Heart Journal. 2020;41(24):2334–5. DOI: 10.1093/eurheartj/ehaa474
6. Bihan H, Heidar R, Beloeuvre A, Allard L, Ouedraogo E, Tatulashvili S et al. Epicardial adipose tissue and severe Coronavirus Disease 19. Cardiovascular Diabetology. 2021;20(1):147. DOI: 10.1186/s12933-021-01329-z
7. Hoori A, Hu T, Al-Kindi S, Rajagopalan S, Wilson DL. Automatic Deep Learning Segmentation and Quantification of Epicardial Adipose Tissue in Non-Contrast Cardiac CT scans. Annual International Conference of the IEEE Engineering in Medicine and Biology Society. 2021;2021:3938–42. DOI: 10.1109/EMBC46164.2021.9630953
8. Commandeur F, Goeller M, Betancur J, Cadet S, Doris M, Chen X et al. Deep Learning for Quantification of Epicardial and Thoracic Adipose Tissue From Non-Contrast CT. IEEE Transactions on Medical Imaging. 2018;37(8):1835–46. DOI: 10.1109/TMI.2018.2804799
9. Begoli E, Bhattacharya T, Kusnezov D. The need for uncertainty quantification in machine-assisted medical decision making. Nature Machine Intelligence. 2019;1(1):20–3. DOI: 10.1038/s42256-018-0004-1
10. Zhao C, Xu Y, He Z, Tang J, Zhang Y, Han J et al. Lung segmentation and automatic detection of COVID-19 using radiomic features from chest CT images. Pattern Recognition. 2021;119:108071. DOI: 10.1016/j.patcog.2021.108071
11. Jocher G, Stoken A, Borovec J, NanoCode012, Chaurasia A, TaoXie et al. ultralytics/yolov5: v5.0 - YOLOv5-P6 1280 models, AWS, Supervise.ly and YouTube integrations. 2021. Av. at: https://zenodo.org/records/4679653
12. Ronneberger O, Fischer P, Brox T. U-Net: Convolutional Networks for Biomedical Image Segmentation. P. 234-241. [DOI: 10.1007/978-3-319-24574-4_28] In: Medical Image Computing and Computer-Assisted Intervention – MICCAI 2015. - Cham: Springer International Publishing, 2015. ISBN: 978-3-319-24573-7
13. Zwanenburg A, Vallières M, Abdalah MA, Aerts HJWL, Andrearczyk V, Apte A et al. The Image Biomarker Standardization Initiative: Standardized Quantitative Radiomics for High-Throughput Image-based Phenotyping. Radiology. 2020;295(2):328–38. DOI: 10.1148/radiol.2020191145
14. Luo C-L, Rong Y, Chen H, Zhang W-W, Wu L, Wei D et al. A Logistic Regression Model for Noninvasive Prediction of AFP-Negative Hepatocellular Carcinoma. Technology in Cancer Research & Treatment. 2019;18:153303381984663. DOI: 10.1177/1533033819846632
15. Suykens JAK, Vandewalle J. Least Squares Support Vector Machine Classifiers. Neural Processing Letters. 1999;9(3):293–300. DOI: 10.1023/A:1018628609742
16. Belgiu M, Drăguţ L. Random forest in remote sensing: A review of applications and future directions. ISPRS Journal of Photogrammetry and Remote Sensing. 2016;114:24–31. DOI: 10.1016/j.isprsjprs.2016.01.011
17. Bahad P, Saxena P. Study of AdaBoost and Gradient Boosting Algorithms for Predictive Analytics. P. 235-244. [DOI: 10.1007/978-981-15-0633-8_22] In: International Conference on Intelligent Computing and Smart Communication 2019. - Singapore: Springer Singapore, 2020. ISBN: 978-9811506321
18. Chen T, Guestrin C. XGBoost: A Scalable Tree Boosting System. P.785-794. [DOI: 10.1145/2939672.2939785] Proceedings of the 22nd ACM SIGKDD International Conference on Knowledge Discovery and Data Mining. - San Francisco California USA: ACM, 2016. ISBN: 978-1-4503-4232-2
19. Sai MJ, Chettri P, Panigrahi R, Garg A, Bhoi AK, Barsocchi P. An Ensemble of Light Gradient Boosting Machine and Adaptive Boosting for Prediction of Type-2 Diabetes. International Journal of Computational Intelligence Systems. 2023;16(1):14. DOI: 10.1007/s44196-023-00184-y
20. Blagus R, Lusa L. Gradient boosting for high-dimensional prediction of rare events. Computational Statistics & Data Analysis. 2017;113:19–37. DOI: 10.1016/j.csda.2016.07.016
21. Ji X, Ma Y, Shi N, Liang N, Chen R, Liu S et al. Clinical characteristics and treatment outcome of COVID-19 patients with stroke in China: A multicenter retrospective study. Phytomedicine. 2021;81:153433. DOI: 10.1016/j.phymed.2020.153433
22. Liang W, Liang H, Ou L, Chen B, Chen A, Li C et al. Development and Validation of a Clinical Risk Score to Predict the Occurrence of Critical Illness in Hospitalized Patients With COVID-19. JAMA Internal Medicine. 2020;180(8):1081–9. DOI: 10.1001/jamainternmed.2020.2033
23. Zhao C, Bai Y, Wang C, Zhong Y, Lu N, Tian L et al. Risk factors related to the severity of COVID-19 in Wuhan. International Journal of Medical Sciences. 2021;18(1):120–7. DOI: 10.7150/ijms.47193
24. Zhang R, Xiao Q, Zhu S, Lin H, Tang M. Using different machine learning models to classify patients into mild and severe cases of COVID-19 based on multivariate blood testing. Journal of Medical Virology. 2022;94(1):357–65. DOI: 10.1002/jmv.27352
25. Li K, Fang Y, Li W, Pan C, Qin P, Zhong Y et al. CT image visual quantitative evaluation and clinical classification of coronavirus disease (COVID-19). European Radiology. 2020;30(8):4407–16. DOI: 10.1007/s00330-020-06817-6
26. Klüner LV, Oikonomou EK, Antoniades C. Assessing Cardiovascular Risk by Using the Fat Attenuation Index in Coronary CT Angiography. Radiology: Cardiothoracic Imaging. 2021;3(1):e200563. DOI: 10.1148/ryct.2021200563
27. Milletari F, Navab N, Ahmadi S-A. V-Net: Fully Convolutional Neural Networks for Volumetric Medical Image Segmentation. 2016 Fourth International Conference on 3D Vision (3DV). P. 565–571. 2016. [DOI: 10.1109/3DV.2016.79]

ISSN 0022-9040. Кардиология. 2024;64(9). DOI: 10.18087/cardio.2024.9.n2685